Modulation of extrasynaptic NMDA receptors by synaptic and tonic zinc

Citation: Anderson, Charles T., Robert J. Radford, Melissa L. Zastrow, Daniel Y. Zhang, Ulf-Peter Apfel, Stephen J. Lippard, and Thanos Tzounopoulos. "Modulation of Extrasynaptic NMDA Receptors by Synaptic and Tonic Zinc." Proc Natl Acad Sci USA 112, no. 20 (May 6, 2015): E2705–E2714.

As Published: http://dx.doi.org/10.1073/pnas.1503348112

Publisher: National Academy of Sciences (U.S.)

Persistent URL: http://hdl.handle.net/1721.1/100585

Version: Final published version: final published article, as it appeared in a journal, conference proceedings, or other formally published context

Modulation of extrasynaptic NMDA receptors by synaptic and tonic zinc

Charles T. Anderson[a], Robert J. Radford[b], Melissa L. Zastrow[b], Daniel Y. Zhang[b], Ulf-Peter Apfel[b], Stephen J. Lippard[b,1], and Thanos Tzounopoulos[a,c,1]

[a]Departments of Otolaryngology and Neurobiology, University of Pittsburgh, Pittsburgh, PA 15261; [b]Department of Chemistry, Massachusetts Institute of Technology, Cambridge, MA 02139; and [c]Whitman Center, Marine Biological Laboratory, Woods Hole, MA 02543

Edited by Robert C. Malenka, Stanford University School of Medicine, Stanford, CA, and approved April 7, 2015 (received for review February 17, 2015)

Many excitatory synapses contain high levels of mobile zinc within glutamatergic vesicles. Although synaptic zinc and glutamate are coreleased, it is controversial whether zinc diffuses away from the release site or whether it remains bound to presynaptic membranes or proteins after its release. To study zinc transmission and quantify zinc levels, we required a high-affinity rapid zinc chelator as well as an extracellular ratiometric fluorescent zinc sensor. We demonstrate that tricine, considered a preferred chelator for studying the role of synaptic zinc, is unable to efficiently prevent zinc from binding low-nanomolar zinc-binding sites, such as the high-affinity zinc-binding site found in NMDA receptors (NMDARs). Here, we used ZX1, which has a 1 nM zinc dissociation constant and second-order rate constant for binding zinc that is 200-fold higher than those for tricine and CaEDTA. We find that synaptic zinc is phasically released during action potentials. In response to short trains of presynaptic stimulation, synaptic zinc diffuses beyond the synaptic cleft where it inhibits extrasynaptic NMDARs. During higher rates of presynaptic stimulation, released glutamate activates additional extrasynaptic NMDARs that are not reached by synaptically released zinc, but which are inhibited by ambient, tonic levels of nonsynaptic zinc. By performing a ratiometric evaluation of extracellular zinc levels in the dorsal cochlear nucleus, we determined the tonic zinc levels to be low nanomolar. These results demonstrate a physiological role for endogenous synaptic as well as tonic zinc in inhibiting extrasynaptic NMDARs and thereby fine tuning neuronal excitability and signaling.

NMDA receptors | zinc | glutamate spillover | zinc dynamics | ratiometric zinc sensors | zinc chelators

In many excitatory neurons, the zinc transporter ZnT3 loads high levels of free (readily chelatable) zinc into glutamatergic vesicles. Synaptic zinc is coreleased with glutamate into the extracellular space in an activity-dependent manner, where it modulates the function of many targets, including ion channels and receptors (1, 2). It is nonetheless controversial whether or not synaptic zinc acts via a classic phasic release mode defined by short-lived, high concentrations of chelatable zinc that diffuse away from the release site (3, 4). The fact that zinc binds with high affinity to many proteins, and the inconsistent measurements of chelatable zinc after synaptic release, ranging from no detectable to 100 μM levels (1), have led to an alternative hypothesis for the mode of synaptic zinc transmission and action. According to this model, rather than being free to diffuse, synaptic zinc is postulated to remain bound to presynaptic membrane or protein structures forming a "veneer" of zinc in the synaptic cleft (5, 6). This so-called zinc veneer model predicts that synaptic zinc modulation is mediated by slow buildup of an extracellular layer of zinc ions during synaptic activity, referred to as tonic zinc signaling.

A recent study suggests a mixed mode of zinc release and action, whereby zinc is phasically released but acts in a tonic-like manner because trains of action potentials are required to inhibit synaptic NMDA receptors (NMDARs) at mossy fiber synapses (7). However, this study directly contradicts previous findings at mossy fiber synapses showing that only a single action potential invading a mossy fiber axon is capable of releasing a sufficient amount of zinc to inhibit NMDARs (8). Such conflicting conclusions prevail in many imaging and electrophysiological studies addressing the mode of mobile zinc transmission and action (5, 7–13), obfuscating the physiological role of zinc in neurons.

The inability to resolve fundamental questions about synaptic zinc transmission is due in part to the lack of zinc-sensing fluorescent probes and zinc-chelating agents optimized for quantifying and interrupting localized, rapidly released synaptic zinc ions. To address the quantitation issue, we synthesized an extracellular ratiometric fluorescent zinc sensor (LZ9) for accurate measurement of chelatable zinc levels. To identify the most appropriate zinc chelator we compared the affinity and kinetics of zinc chelation of three widely-used extracellular zinc chelators, ZX1, CaEDTA, and tricine (7, 8). We subsequently chose ZX1 and applied it together with LZ9 in electrophysiological, laser-based glutamate uncaging and imaging investigations of mobile zinc in WT and genetically modified mice that lack ZnT3, the transporter that loads presynaptic vesicles with zinc. We studied zinc-dependent neuronal activity in cartwheel cells, a class of inhibitory interneurons in the molecular layer of the dorsal cochlear nucleus (DCN) that receive glutamatergic input from synaptic zinc-rich parallel fibers (13–15). The DCN has a cerebellum-like organization, and cartwheel cells share common morphological, ontological, and physiological features with cerebellar neurons (15, 16). One of the major physiological properties of cerebellar molecular layer interneurons is the expression of extrasynaptic NMDARs that are activated by glutamate spillover in response to short trains of parallel fiber action potentials

Significance

As an essential element for living organisms, zinc is a cofactor in many enzymes and regulatory proteins. After the surprising discovery of mobile zinc in synaptic vesicles throughout many areas of the brain, numerous investigators have studied its possible roles during neurotransmission. Nonetheless, knowledge of the physiology of zinc at the synapse is still in its infancy. Here, we show that synaptic and tonic zinc inhibit extrasynaptic NMDA receptors (NMDARs), which are widely distributed in the CNS and are important for normal and pathological excitatory signaling. Our work indicates that this newly discovered interaction between zinc and extrasynaptic NMDARs can provide a general mechanism for controlling neuronal excitability in the CNS.

Author contributions: C.T.A., R.J.R., M.L.Z., S.J.L., and T.T. designed research; C.T.A., R.J.R., M.L.Z., D.Y.Z., and T.T. performed research; R.J.R., D.Y.Z., U.-P.A., and S.J.L. contributed new reagents/analytic tools; C.T.A., R.J.R., M.L.Z., D.Y.Z., and T.T. analyzed data; and C.T.A., R.J.R., M.L.Z., S.J.L., and T.T. wrote the paper.

The authors declare no conflict of interest.

This article is a PNAS Direct Submission.

[1]To whom correspondence may be addressed. Email: lippard@mit.edu or thanos@pitt.edu.

This article contains supporting information online at www.pnas.org/lookup/suppl/doi:10.1073/pnas.1503348112/-/DCSupplemental.

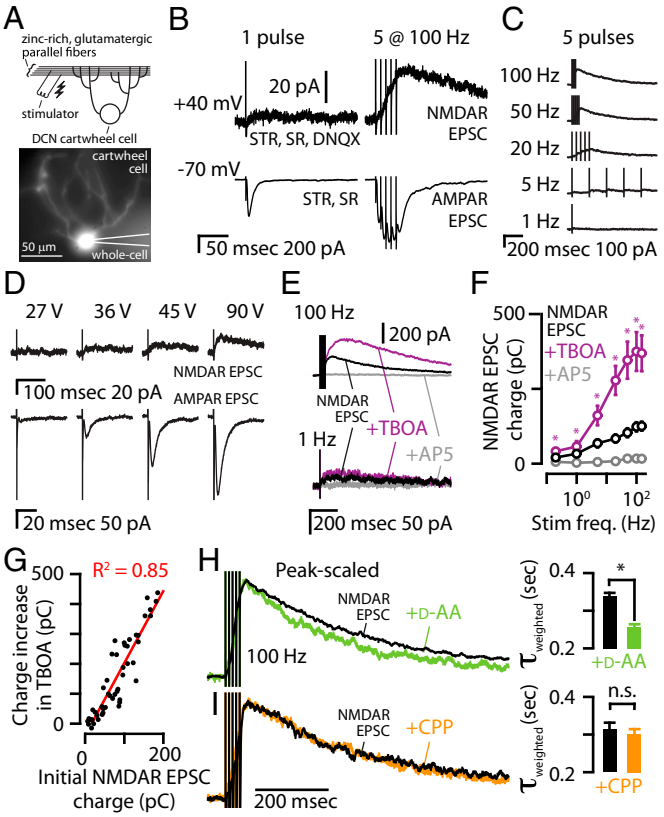

Fig. 1. In DCN cartwheel cells, short trains of parallel fiber stimulation evoke NMDAR EPSCs mediated by extrasynaptic NMDARs. (*A*) (*Top*) Cartoon showing experimental setup with stimulating electrode in the synaptic zinc-rich region of the DCN and a cartwheel cell. (*Bottom*) Epifluorescence showing the dendritic arbor of this cartwheel cell filled with Alexa-594 during whole-cell recording. (*B*) At −70 mV, a single electrical pulse caused a robust AMPAR EPSC, but at +40 mV the same pulse did not reveal a robust NMDAR EPSC. In the same cartwheel cell, five pulses delivered at 100 Hz caused AMPAR EPSC summation at −70 mV and a buildup of an NMDAR EPSC at +40 mV. AMPAR EPSCs were pharmacologically isolated with blockers of $GABA_A$Rs (SR95531, SR, 20 µM) and GlyRs (strychnine, STR, 1 µM). NMDAR EPSCs were isolated by also blocking AMPARs (DNQX, 20 µM) and relieving the NMDAR magnesium block by changing the command potential to +40 mV. To confirm that the EPSCs were mediated by NMDARs, at the end of each experiment, the NMDAR antagonist AP5 (50 µM) was applied. (*C*) Example of isolated NMDAR EPSCs in response to increasing stimulus frequency. (*D*) Single electrical pulses elicited an AMPAR EPSC at lower stimulus intensity compared with the stimulus intensity required for eliciting an NMDAR EPSC. (*E*) Representative traces showing that TBOA (50 µM) potentiated the NMDAR EPSC following 100-Hz stimulus trains but had a smaller effect on the NMDAR EPSC following a 1-Hz stimulus train. (*F*) Group data showed that TBOA significantly potentiated the NMDAR EPSC (paired *t* tests, $n = 7$). (*G*) The increase in charge of the NMDAR EPSC in TBOA was significantly correlated with the initial NMDAR EPSC charge, $P = 0.0001$. (*H*) (*Left*) Peak-scaled NMDAR EPSCs following a five-pulse, 100-Hz train stimulus showed that D-AA (70 µM) sped the decay tau. (*Right*) Group data showing that D-AA significantly sped the decay tau ($P = 0.01$, paired *t* test, $n = 4$). (*I*) (*Left*) Peak-scaled NMDAR EPSCs following a five-pulse, 100-Hz train stimulus showed that CPP (1 µM) did not affect the decay tau. (*Right*) Group data showing that CPP did not significantly speed the decay tau ($P = 0.16$, paired *t* test, $n = 5$). Error bars represent SEM. Detailed values are given in *SI Materials and Methods, Values for Main Figures*.

(17, 18). Because zinc inhibits NMDARs with high affinity (19, 20), and because synaptic zinc must act in a phasic manner and diffuse away from the release site to inhibit extrasynaptic NMDARs, we investigated whether synaptic zinc modulates extrasynaptic NMDARs in cartwheel cells.

Results

Activation of Extrasynaptic NMDARs by Glutamate Spillover. First, we characterized the activation of extrasynaptic NMDARs in cartwheel cells (Fig. 1*A*). A single stimulus to parallel fibers caused robust AMPA receptor (AMPAR) excitatory postsynaptic currents (EPSCs) but failed to elicit or elicited very weak NMDAR EPSCs (Fig. 1*B*, *Left*). Because AMPARs have a lower affinity for glutamate than NMDARs (21), robust AMPAR EPSCs from a single stimulus suggests that AMPARs are closer to the release sites than NMDARs. Consistent with this hypothesis, a 100-Hz stimulus train of five pulses caused NMDAR activation at +40 mV (Fig. 1*B*, *Right*), and summation of AMPAR EPSCs at −70 mV, suggesting buildup of glutamate in the extracellular space during the train and activation of extrasynaptic NMDARs by glutamate spillover to extrasynaptic locations (17, 22). Consistent with this conclusion, increasing the stimulus frequency over a wide range of frequencies resulted in larger NMDAR EPSCs (Fig. 1 *B* and *C*). Whereas an NMDAR EPSC was activated at stimulus frequencies ≥5 Hz, increasing the stimulus intensity also revealed a slow NMDAR EPSC in response to a single electrical pulse, but always at intensities higher than those required for AMPAR EPSCs (Fig. 1*D*). This result suggests that synchronous activation of a larger number of fibers (synapses) leads to "pooling" of glutamate that is capable of activating extrasynaptic NMDARs. Because even weak stimuli probably activate more than one parallel fiber in the DCN (23), pooling of glutamate in response to a single stimulus is consistent with the small NMDAR EPSCs following a single electrical pulse. Together, these results suggest that low-frequency activation of small numbers of parallel fibers generate AMPAR-only EPSCs, but activation of a larger number of fibers (pooling) and/or facilitation of glutamate release (spillover) generate extrasynaptic NMDAR EPSCs.

To further evaluate this hypothesis, we used DL-threo-β-benzyloxyaspartate (TBOA), a glutamate transporter inhibitor that blocks glutamate clearance and enhances glutamate spillover and pooling. TBOA (50 µM) increased the charge carried by NMDAR EPSCs (Fig. 1 *E* and *F*), indicating that glutamate spillover is activating extrasynaptic NMDARs. Consistent with glutamate spillover that depends on the amount of released glutamate (17), the magnitude of the effect of TBOA was correlated with the initial NMDAR-mediated charge (Fig. 1*G*). To further confirm glutamate spillover and pooling at parallel fiber to cartwheel cell synapses, we examined the effect of D-α-amino adipate (D-AA), a low-affinity NMDAR antagonist with the ability to inhibit NMDAR EPSCs, depending on the concentration of glutamate. When glutamate spillover occurs, D-AA is expected to preferentially block the slower components of the NMDAR EPSC, which are activated by slower glutamate transients and lower glutamate concentrations (24, 25). Consistent with the spillover hypothesis, D-AA (70 µM) decreased the amplitude and sped up the decay of NMDAR EPSCs (Fig. 1*H*). To determine whether faster kinetics reflect improved space clamp of the smaller EPSCs in D-AA, we tested the effect of the high-affinity NMDAR antagonist 3-[(+)-2-carboxypiperazin-4-yl]-propyl-1-phosphonic acid (CPP, 1 µM), which caused a similar decrease in the EPSC. Unlike D-AA, CPP did not affect the decay kinetics of NMDAR EPSCs, further validating that the faster kinetics observed in D-AA are due to glutamate spillover and reduced glutamate concentrations at extrasynaptic sites and not to improved space clamp of the smaller EPSCs in D-AA. To confirm that glutamate spillover activates NMDARs at more physiologically relevant temperatures, we measured the effect of D-AA on NMDAR EPSCs at 32 °C. At 32 °C the NMDAR EPSC decayed more rapidly than at room temperature (Fig. S1*A*). Nonetheless, at 32 °C, D-AA sped the decay kinetics of the NMDAR EPSC to the same extent as at room temperature (Fig. S1 *A* and *B*), indicating that activation of NMDARs by glutamate spillover occurs at more physiological

temperatures. Moreover, consistent with spillover-mediated recruitment of extrasynaptic NMDARs under more physiological conditions, a single stimulus evoked NMDAR EPSCs at 32 °C only at intensities higher than those required for AMPAR EPSCs (Fig. S1*C*). Together, our results indicate that, in response to short trains of presynaptic stimulation, NMDAR EPSCs recorded in somata of cartwheel cells are mostly mediated by extrasynaptic NMDARs that are activated by glutamate spillover.

ZX1 Is More Efficient Than Tricine or CaEDTA in Chelating Fast Zinc Transients from Nanomolar Affinity Zinc-Binding Sites. To investigate whether synaptic zinc inhibits extrasynaptic NMDARs, we first required a rapid zinc chelator to intercept this ion before it reaches these receptors. To determine the most appropriate extracellular chelator, we compared the affinity and rapidity for zinc chelation of three widely-used extracellular zinc chelator candidates, CaEDTA, tricine, and ZX1 (Fig. 2*A*). Previous studies compared CaEDTA and tricine and, based on simulations, concluded that tricine is much faster than CaEDTA and therefore more appropriate for intercepting fast synaptic zinc transients (1). In addition, kinetic studies of zinc binding to CaEDTA or ZX1, by competition with the ditopic zinc sensor ZP3, revealed that ZX1 could bind zinc faster than CaEDTA (8). Importantly, the use of ZX1 vs. CaEDTA was essential in demonstrating novel roles of synaptic zinc in mossy fiber long-term potentiation (LTP) (8). However, no study has compared all three chelators and it is therefore unclear whether tricine or ZX1 is more appropriate for studying the roles of mobile zinc in neurotransmission. This choice is an important one for elucidating the functions of synaptic zinc and is highlighted by the discrepancy observed between two recent studies. An investigation using tricine concluded that short trains of action potentials are needed for zinc modulation of NMDARs in mossy fiber synapses (7), but previous work using ZX1, in the same synapses, revealed that a single action potential is capable of evoking zinc-mediated modulation of NMDARs (8).

To compare the affinity for zinc among the chelators, we performed potentiometric titrations to derive dissociation constants ($K_{d\text{-}Zn}$) for tricine that could be compared with previously reported data on CaEDTA and ZX1 (Fig. S2). The derived apparent $K_{d\text{-}Zn}$ value, at pH 7.4, $I = 0.1$ M, and 25 °C, is 2 nM for CaEDTA and 1 nM for ZX1 (8, 26). We found that the apparent $K_{d\text{-}Zn}$ under the same conditions was 2.8 μM for the mixture of 1:1 and 1:2 zinc:tricine complexes present in solution at pH 7.4 (Fig. S2), which is consistent with previous empirical calculations (19). Having confirmed ZX1 and CaEDTA both have much higher affinity for zinc than tricine, we next investigated the metal binding kinetics for the three chelators. For these experiments, we took advantage of fluorescent zinc sensors with known zinc-binding affinities. Addition of 100 μM CaEDTA or 100 μM ZX1 to a solution of 1 μM Zn_2ZPP1 [$K_{d\text{-}Zn}$ = 15.6 nM (27)] completely eliminates zinc-induced fluorescence emission (Fig. 2*B*). However, even high very levels of tricine (100 mM) were unable to completely attenuate the fluorescence (Fig. 2*B*). Notably, 10 mM tricine, the concentration used in previous electrophysiological studies for probing the role of synaptic zinc (7), only reduced the fluorescence by ∼30% (Fig. 2*B*). This result suggests that 10 mM tricine is unable to efficiently compete with high-affinity/low-nanomolar zinc-binding sites, such as the high affinity zinc-binding site found in GluN2A-containing NMDARs (19).

To measure the rate of zinc binding to the chelators, we performed stopped-flow kinetics experiments, where the rate of fluorescence reduction arises from removal of zinc from the prebound zinc–sensor complex by the chelator. For these experiments, we used a weaker-affinity sensor, 2,4-DPA-7-hydroxycoumarin-3-carboxylic acid, or 3-CO_2H CM2 ($K_{d\text{-}Zn}$ = 5 μM, Fig. 2*C*

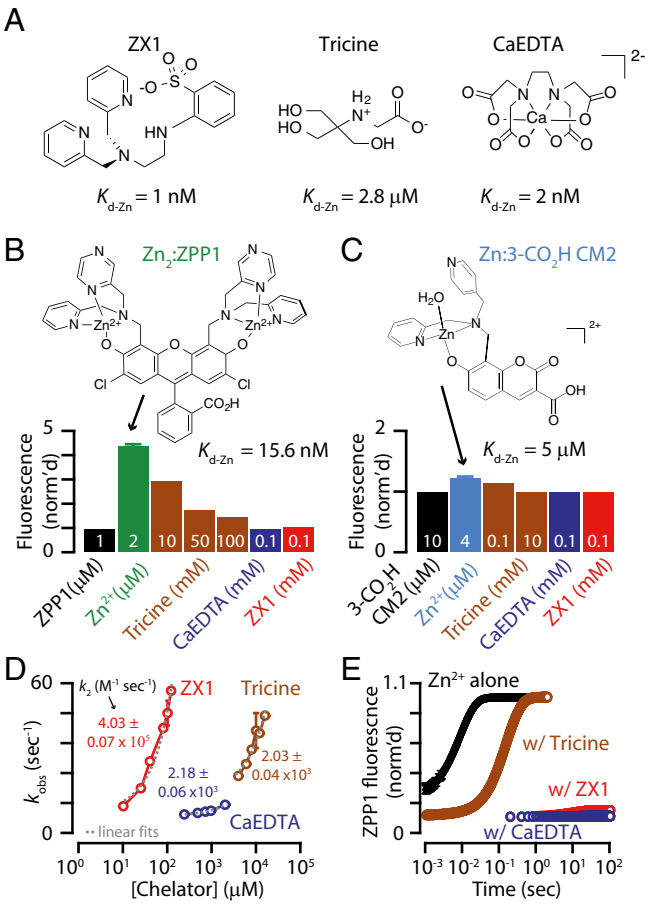

Fig. 2. Kinetics and zinc binding for extracellular chelators, ZX1, tricine, and CaEDTA. (*A*) Line drawings of extraceullar zinc chelators at pH 7.4. (*B*) Normalized fluorescence signals for addition of each chelator to 1 μM Zn_2ZPP1 at pH 7.4 in buffer [50 mM piperazine-*N*,*N*′-bis(2-ethanesulfonic acid) (PIPES) and 100 mM KCl]. λ_{ex} = 495 nm, λ_{em} = 500–650 nm. Integrated fluorescence signals were normalized to the fluorescence emission of 1 μM ZPP1; 10–100 mM tricine ($K_{d\text{-}Zn}$ = 2.8 μM) attenuated, but did not abolish, zinc-induced fluorescence turn-on (ZPP1 $K_{d\text{-}Zn}$ = 15.6 nM). The high-affinity chelators, ZX1 ($K_{d\text{-}Zn}$ = 1 nM) and CaEDTA ($K_{d\text{-}Zn}$ = 2 nM), can chelate zinc from ZPP1, as evidenced by complete fluorescence turn-off. (*C*) Normalized fluorescence signals for addition of chelators to 4 μM Zn(3-CO_2H CM2) (a water molecule was added to complete the coordination sphere of zinc because the structure is unknown) at pH 7.4 in 50 mM PIPES and 100 mM KCl. λ_{ex} = 355 nm, λ_{em} = 400–550 nm. Integrated fluorescence signals were normalized to the fluorescence of 10 μM 3-CO_2H CM2; 10 mM tricine, and 100 μM each of ZX1 and CaEDTA, could completely remove zinc from this relatively low affinity sensor ($K_{d\text{-}Zn}$ = 5 μM). (*D*) Plots of observed pseudo-first-order rate constants for the addition of chelator to a solution of 2 μM Zn(3-CO_2H CM2) (with 8 μM excess 3-CO_2H CM2) as measured by stopped flow fluorescence (λ_{ex} = 355 nm, λ_{em} = 400–700 nm) at pH 7.0 in 50 mM PIPES and 100 mM KCl. Fluorescence turn-off reflects zinc binding by the chelators, ZX1, tricine, and CaEDTA. Varying [ZX1] from 10 to 120 μM yielded rapid turn-off kinetics with observed rates up to 57 s^{-1}. Tricine concentrations nearly 100-fold higher resulted in similar rates, up to 47 s^{-1} for 16 mM tricine. Varying [CaEDTA] from 0.24 to 2 mM yielded relatively low rates up to 11.3 s^{-1}. The second-order rate constants were derived from linear fits of k_{obs} vs. [chelator]. (*E*) Rate and extent of fluorescence turn-on for a solution of 1 μM ZPP1 upon addition of 50 μM zinc, or 50 μM zinc + chelator (100 μM ZX1, 10 mM tricine, or 125 μM CaEDTA), as measured by stopped flow fluorescence (λ_{ex} = 495 nm, λ_{em} = 495–700 nm) at pH 7.0 in 50 mM PIPES and 100 mM KCl. In the presence of excess zinc, ZPP1 turns on rapidly and completely (time to completion ∼0.02 s). When the same amount of zinc is added in the presence of excess tricine, the rate of zinc binding is diminished ∼30-fold (time to completion ∼0.6 s), but not prevented. Both ZX1 and CaEDTA premixed with zinc prevented turn-on of ZPP1, showing that only the higher-affinity zinc chelators can compete with nanomolar zinc-binding sites. Data are normalized to the fluorescence level of 1 μM of Zn_2ZPP1. Error bars represent SD. Detailed values are given in *SI Material and Methods, Values for Main Figures*.

and Fig. S3), which permitted complete turn-off of the zinc-induced fluorescence by 100 μM ZX1, 100 μM CaEDTA, and 10 mM tricine (Fig. 2*C*). We added various chelator concentrations to remove zinc from the preformed zinc-sensor complex, which decreased the fluorescence to the initial zinc-free value of the sensor (Fig. S4). The range of chelator concentrations was chosen based on those applied in electrophysiological experiments (7, 8) (Fig. 2*D*). An overlay of selected pseudo-first-order kinetic traces for each chelator at pH 7.0 and 7.4 revealed that ZX1 and tricine both chelated zinc rapidly, whereas CaEDTA was slower (Fig. S4 *D* and *E*). Plotting each observed pseudo-first-order rate constant as a function of chelator concentration afforded second-order rate constants (k_2) for each competition (Fig. 2*D*). The resulting k_2 value for ZX1 is 4.03 (± 0.07) × 10^5 $M^{-1}{\cdot}s^{-1}$, 200-fold larger than those for tricine and CaEDTA (Fig. 2*D*). These values demonstrate both the slower first-order chelation rate of CaEDTA and the weaker zinc-binding affinity of tricine.

Next, we took an alternative approach to examine the kinetics of zinc-induced sensor turn-on in the presence of different chelators. Solutions of 50 μM zinc alone and in the presence of chelators (10 mM tricine, 100 μM ZX1, or 125 μM CaEDTA) were added to a solution of 1 μM ZPP1 (low-nanomolar affinity) and the fluorescence turn-on was measured by stopped flow spectroscopy. Maximal fluorescence of ZPP1 was observed in 0.02 s upon addition of 50 μM zinc (Fig. 2*E* and Fig. S5 *A* and *B*). In the presence of 10 mM tricine, zinc binding was attenuated briefly, but maximal fluorescence was achieved in 0.6 s (Fig. 2*E* and Fig. S5*C*). In the presence of 100 μM ZX1 or 125 μM CaEDTA, however, minimal fluorescence turn-on was observed even over 100 s (Fig. 2*E* and Fig. S5 *D* and *E*). These results further reveal the inability of 10 mM tricine to effectively compete with nanomolar affinity zinc-binding sites but do show that 10 mM tricine delays zinc binding for about 0.4 s. Conversely, ZX1 binds zinc rapidly and completely prevents zinc binding to nanomolar affinity sites at relatively low concentrations and over longer time scales. Collectively, both ZX1 and tricine bind zinc more rapidly than CaEDTA, but tricine cannot compete effectively for zinc binding to nanomolar affinity sites. These results clearly reveal that ZX1 is the most appropriate chelator for investigating the effects of fast, transient elevations of zinc on synaptic targets with nanomolar affinity, such as GluN2A-containing NMDARs.

ZnT3-Dependent Synaptic Zinc Inhibits Extrasynaptic NMDARs. Given the 1 nM affinity for zinc and the fast zinc-chelating kinetics of ZX1 (Fig. 2), we used this construct to chelate zinc and test whether synaptic zinc modulates extrasynaptic NMDARs. We recorded NMDAR EPSCs at positive potentials where voltage-independent, physiologically relevant zinc modulation occurs with high affinity in GluN2A-containing NMDARs (7, 19, 20, 28). Application of ZX1 (100 μM) increased the peak amplitude of NMDAR EPSCs evoked by five pulses at 5 and 20 Hz, a result consistent with zinc-mediated inhibition of extrasynaptic NMDARs (Fig. 3 *A*–*C*). When we recorded NMDAR EPSCs at hyperpolarizing potentials, we did not reveal any additional ZX1 potentiation (Fig. S6*A*). The lack of zinc modulation of the voltage-dependent, low-affinity zinc-binding site on NMDARs is consistent with zinc-mediated modulation of the high-affinity GluN2A site (19, 29).

To confirm the origin of this extracellular zinc-mediated inhibition of extrasynaptic NMDARs, we tested the effects of ZX1 on NMDAR EPSCs in DCN slices from ZnT3 KO mice (30). Zinc chelation did not potentiate extrasynaptic NMDARs in ZnT3 KO mice, confirming that synaptic/ZnT3-dependent zinc inhibits extrasynaptic NMDARs (Fig. 3 *A*–*C*).

Although in vivo recordings from DCN granule cells, the source of parallel fibers, have not been obtained, cerebellar granule cells fire action potentials at rates of up to several hundred hertz in response to mossy fiber input (31, 32). Given the strong parallels between the cerebellum and DCN, the stimulation protocols of a few pulses at frequencies from 5 to 150 Hz, which we used in our study (see Figs. 3, 5, and 6), fall well within the physiological range of parallel fiber activity. Moreover, at 32 °C, ZX1 potentiated NMDAR EPSCs to a similar degree, indicating that zinc modulates extrasynaptic NMDARs at more physiological temperatures (Fig. S6*B*).

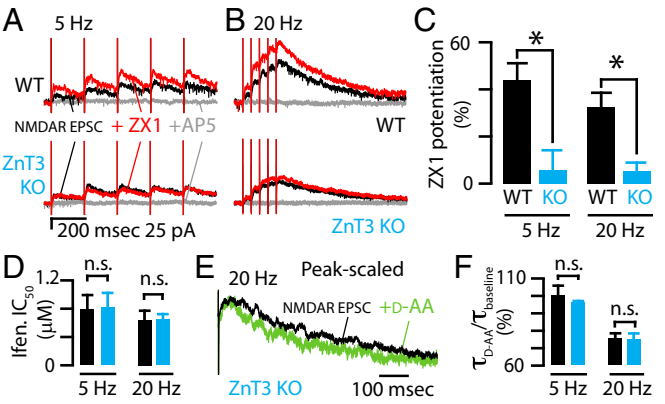

Fig. 3. Synaptic (ZnT3-dependent) zinc inhibits extrasynaptic NMDARs. (*A*) (*Top*) A 5-Hz stimulus train was delivered to DCN parallel fibers while recording from a cartwheel cell to evoke pharmacologically isolated NMDAR EPSCs (in the presence of SR95531, strychnine, DNQX). The addition of the fast extracellular chelator ZX1 (100 μM) potentiated this NMDAR EPSC (red), and the addition of AP5 (gray) (50 μM) abolished the response. (*Bottom*) In a cartwheel cell from a ZnT3 KO mouse, the addition of ZX1 had no effect on this NMDAR EPSC. (*B*) Same experiment as in *A*, but with a 20-Hz stimulus train. (*C*) Quantification of the effect of zinc chelation showing that the peak amplitude of NMDAR EPSCs recorded from WT mice were significantly potentiated by ZX1 and that those from ZnT3 KO were not potentiated by ZX1 ($n = 8$ for WT; $n = 6$ for ZnT3 KO; WT vs. ZnT3 KO: 5 Hz, $P = 0.008$; 20 Hz, $P = 0.01$, *t* tests). (*D*) The IC_{50} of ifenprodil for NMDARs activated by different stimulus trains were not different between WT and ZnT3 KO ($n = 5$ for both; 5 Hz: $P = 0.93$; 20 Hz: $P = 0.99$, *t* tests). (*E*) Example trace showing that D-AA sped the decay kinetics of the NMDAR EPSC in ZnT3 KO mice. Traces were aligned to the last stimulus artifact of the train. (*F*) Group data showed that the effect of D-AA on the decay kinetics of NMDAR EPSCs was not different between WT and ZnT3 KO ($\tau_{D\text{-}AA}/\tau_{baseline}$, 5 Hz: WT vs. KO, $n = 4$, $P = 0.86$, rank sum test; 20 Hz: WT vs. KO, $P = 0.81$, *t* test). Error bars represent SEM. Detailed values are given in *SI Material and Methods, Values for Main Figures*.

Most native NMDARs are composed of two GluN1 and two GluN2 subunits (33). Because GluN2A-containing NMDARs (GluN1/GluN2A diheteromers and GluN1/GluN2A/GluN2B triheteromers) have nanomolar affinity for zinc, whereas GluN1/GluN2B diheteromers have micromolar affinity for zinc (19, 20, 34, 35), we tested whether the inability of ZX1 to potentiate extrasynaptic NMDARs in ZnT3 KO mice was due to a different proportion of GluN2A vs. GluN2B subunits between WT and KO mice. Because GluN2A subunits are differentially sensitive to antagonists compared with GluN2B subunits (20), we compared the pharmacological profile of NMDAR EPSCs in WT and ZnT3 KO mice in the presence of 100 μM ZX1 (see *SI Materials and Methods* for details). The inhibitory effect of the GluN2B-selective antagonist ifenprodil (IC_{50} values and percent maximal inhibition) was indistinguishable between WT and ZnT3 KO mice (Fig. 3*D* and Table S1), indicating no difference between the proportions of GluN2A vs. GluN2B subunits in these animals. Therefore, the differential ZnT3-dependent inhibition of NMDARs between WT and KO mice is probably due to the absence of synaptic zinc in KO mice, and not to a change in the relative contribution of GluN2A vs. GluN2B subunits in the NMDAR EPSCs in the ZnT3 KO.

Additionally, changes in the synaptic properties of parallel fibers synapses between WT and ZnT3 KO mice could affect glutamate levels and thus lead to differential glutamate spillover between WT and ZnT3 KO mice. However, previous work has established that the quantal release properties of DCN parallel fiber synapses, namely, the miniature EPSC frequency, amplitude, rise time, and decay time, the baseline release probability, and the short-term plasticity (paired-pulse ratio), are not different between WT and ZnT3 KO (13). Importantly, glutamate spillover, measured by the effect of D-AA on NMDAR EPSC decay kinetics, was also indistinguishable between WT and ZnT3 KO mice (Fig. 3 *E* and *F* and Table S1). Therefore, glutamate release and spillover are not altered in ZnT3 KO mice. Together, these results indicate that vesicular, ZnT3-dependent zinc inhibits extrasynaptic NMDARs.

ZnT3-Independent Tonic Zinc Levels Are Nanomolar. ZX1 potentiation of extrasynaptic NMDAR EPSCs could indicate that chelation of synaptically (phasically) released zinc removes extrasynaptic NMDAR inhibition by the metal ion. Alternatively, there might be a tonic level of ZnT3-dependent zinc, arising from spontaneous release of presynaptic vesicles, that inhibits extrasynaptic NMDARs and is independent of synaptic stimulation. To differentiate between these two hypotheses, we quantified the concentration and ZnT3 dependence of tonic zinc. If ZnT3-dependent tonic zinc levels mediate extrasynaptic NMDAR inhibition, we expect them to be significantly smaller in the ZnT3 KO.

To quantify the tonic zinc levels in acute brain slices, we designed a new extracellular ratiometric fluorescent zinc sensor, termed LZ9. Ratiometric probes quantify zinc levels in a manner that is independent of probe concentration. Furthermore, in contrast to intensity-based sensors, ratiometric probes control for instrument variability and background noise, making them less prone to artifacts. LZ9 is composed of the zinc-insensitive red fluorophore lissamine rhodamine B (LRB) linked to a zinc-sensitive green fluorophore [ZP1 (36)] by a nine-residue-long polyproline helix (Fig. 4*A* and Fig. S7 *A* and *B*). Blue illumination excites primarily ZP1 and the fluorescence emission in response to blue light is therefore zinc-sensitive. Interleaved green illumination excites primarily LRB, resulting in zinc-insensitive fluorescence (Fig. 4 *B* and *C*, Fig. S7 *A* and *B*, and Table S2). The ratio of these two fluorescent signals is the ratiometric zinc signal (R) (Fig. S7*C*; see *SI Materials and Methods* for details). LZ9 is selective for zinc ions and it binds zinc with an apparent dissociation constant ($K_{d\text{-}Zn}$) of 0.57 nM (Fig. S7 *D* and *E* and Table S2). After confirming that LZ9 is cell-impermeant (Fig. S7 *F* and *G*), we tested whether LZ9 detects changes in extracellular zinc levels. To do so, we evoked synaptic zinc release from the DCN and measured the change in fluorescence with a multiplexed imaging approach (Fig. 4*C*). Consistent with anatomical studies (37), the stimulus-evoked, ratiometric response of LZ9 (2 μM) was restricted to the molecular layer of the DCN, which is the location of zinc-rich parallel fibers (Fig. 4*D*). The addition of ZX1 attenuated the ratiometric change in fluorescence intensity, confirming that the fluorescence response was due to alterations in extracellular zinc levels following synaptic release (Fig. 4*E*). Moreover, no stimulus-evoked change in LZ9 fluorescence was observed in DCN slices from ZnT3 KO mice (Fig. 4*F*), revealing that the evoked signal is ZnT3-dependent and that LZ9 fluorescence is not due to protonation under our conditions (38). These results show that LZ9 is effective and selective for measuring extracellular zinc signals and therefore well suited for quantifying extracellular zinc levels in the DCN.

To quantify tonic zinc levels in DCN slices from WT and ZnT3 KO mice, we incubated the slices in ACSF containing LZ9 (2 μM), measured zinc-mediated fluorescence, and then used the equation shown in Fig. 4*H* to convert fluorescence ratios to zinc concentration (39). After reaching a stable (tonic) baseline

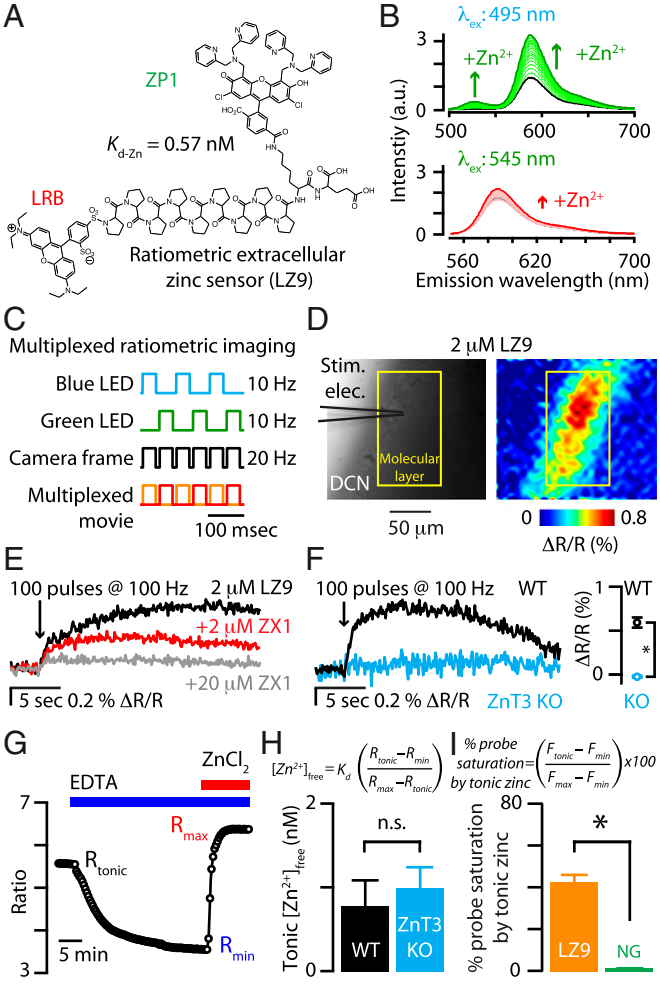

Fig. 4. Novel ratiometric zinc probe detects changes in extracellular free zinc and reveals ZnT3-independent, low-nanomolar tonic zinc levels. (*A*) Chemical structure of the LZ9 ratiometric zinc sensor. This molecule features a zinc-sensitive green fluorophore (ZP1), linked to a zinc-insensitive red fluorophore (LRB) via a nine-residue polyproline linker. (*B*) (*Top*) Change in fluorescence intensity of a 1 μM solution of LZ9 in buffer (50 mM PIPES and 100 mM KCl, pH 7), when exciting ZP1 at 495 nm, upon addition of $ZnCl_2$. (*Bottom*) Fluorescence intensity of the same solution when exciting LRB at 545 nm. (*C*) Blue and green light-emitting diode (LED) illumination were synchronized with the exposure times of a CCD camera: Every other frame used either blue or green excitation. A dual-band green/red Pinkel filter set with appropriate pass bands separated the two excitation and two emission colors (*SI Materials and Methods*). The resulting multiplexed movie was split into the zinc-sensitive orange channel (combined green and red emission) and the zinc-insensitive red channel, each with a 10-Hz frame rate. (*D*) Electrical stimulation of the molecular layer resulted in increased fluorescence from LZ9 that was restricted to the location of the zinc-rich parallel fibers. (*E*) Representative LZ9 fluorescence responses from a WT mouse showing that parallel fiber stimulation (100 pulses at 100 Hz) generates a ratiometric fluorescent signal that is attenuated by ZX1. (*F*) (*Left*) Representative LZ9 fluorescence responses from a WT and a ZnT3 KO mouse showing that parallel fiber stimulation (100 pulses at 100 Hz) does not generate a ratiometric fluorescent signal in the ZnT3 KO mouse, whereas the same stimulation generates a robust signal in the WT mouse. (*Right*) Mean fluorescence response from WT and ZnT3 KO mice ($n = 11$ for WT; $n = 5$ for KO, WT vs. ZnT3 KO, $P = 0.0002$, rank sum test). (*G*) Time course of LZ9 ratiometric response showing tonic fluorescence (R_{tonic}), minimum fluorescence (R_{min}) following the addition of 4.5 mM EDTA ($K_{d\text{-}Zn}$ = 40 fM), and maximum fluorescence (R_{max}) following the addition of 5 mM $ZnCl_2$. (*H*) Conversion of ratiometric signals into free zinc concentrations indicated that tonic zinc levels are not ZnT3-dependent ($n = 5$ for WT; $n = 6$ for ZnT3 KO; WT vs. ZnT3 KO, $P = 0.6$, t test). (*I*) Mean percent probe saturation by tonic zinc for LZ9 and Newport Green (NG) ($n = 11$ for LZ9; $n = 4$ for NG, $P = 0.001$, t test). Error bars represent SEM. Detailed values are given in *SI Material and Methods, Values for Main Figures*.

fluorescence (R_{tonic}), we obtained R_{min} by zinc chelation with EDTA (4.5 mM), a high-affinity zinc chelator ($K_{d\text{-}Zn}$ = 40 fM) (Fig. 4*G*). Although EDTA chelates tonic zinc as well calcium, magnesium, and other divalent metal ions in the extracellular space, the fluorescence of LZ9 is only sensitive to zinc (Fig. S7*E*). Therefore, the use of EDTA for estimating R_{min} does not compromise the calculation of tonic zinc levels. Moreover, because EDTA has femtomolar affinity for zinc, it is able to remove tonic zinc from LZ9, which has a subnanomolar affinity (Fig. S7*D*). EDTA therefore provides an accurate measurement of R_{min} in the presence of LZ9. R_{max} was obtained by saturating the probe with $ZnCl_2$ (5 mM, Fig. 4*G*). Conversion of ratios to tonic zinc levels revealed that WT and ZnT3 KO DCN slices had similar extracellular concentrations of tonic zinc of about 1 nM (Fig. 4*H*). Because the dynamic range of the probe (see *SI Materials and Methods* for details) is the same in the slice and the cuvette (81 ± 5% vs. 78 ± 4%, P = 0.4), we conclude that the out-of-focus probe is not saturated in the slice and it therefore does not distort our measurements. Moreover, because Newport Green (2 μM), a fluorescent sensor with lower affinity for zinc ($K_{d\text{-}Zn}$ = 1 μM), is significantly less saturated by tonic zinc levels (Fig. 4*I*), we conclude that the $K_{d\text{-}Zn}$ of LZ9 is not setting tonic zinc levels, but rather, LZ9 is reporting ~1 nM tonic zinc levels. Together, these results demonstrate that the difference in ZX1 potentiation of extrasynaptic NMDAR EPSCs between WT and ZnT3 KO mice (Fig. 3 *A–C*) is not a consequence of tonic, ZnT3-dependent zinc levels but rather is due to phasic, stimulus-driven release of synaptic zinc in WT mice.

These findings establish synaptic zinc as a neuromodulator that, in response to synaptic stimulation, is phasically released and diffuses to extrasynaptic sites. We thereby resolve a controversy about the ability of synaptic zinc to be phasically released. Importantly, these results provide evidence for synaptic zinc as an endogenous modulator of extrasynaptic NMDARs. Previous studies revealed that synaptic zinc modulates synaptic NMDARs (7, 8, 12, 28) and that extrasynaptic NMDARs are functionally distinct from synaptic NMDARs (40). In this context, the present results differentiate novel physiological roles for synaptic and tonic zinc in modulating extrasynaptic NMDAR-mediated signaling.

Tonic, ZnT3-Independent Zinc Modulates Extrasynaptic NMDARs. To determine whether synaptic zinc modulates extrasynaptic NMDARs during higher, but physiological (31, 32) levels of presynaptic activity, we used the same number of pulses but with higher-frequency stimulus trains (five pulses at 100 or 150 Hz). During higher-frequency trains, ZX1 potentiated NMDAR EPSCs in WT mice, but to a lesser extent (Fig. 5 *A–C*). The differential effects of synaptic zinc during high vs. low frequencies is not due to differences in the proportions of GluN2A vs. GluN2B subunits recruited at the different frequencies, for no differences in pharmacological sensitivity of NMDAR EPSCs were observed (Table S1). Moreover, at 32 °C, ZX1 had a similar effect in potentiating NMDAR EPSCs (Fig. S8), indicating similar modulation of NMDARs by zinc spillover at more physiological temperatures. Together, these results suggest that, although glutamate activates more extrasynaptic NMDARs at higher frequencies (Fig. 1 *C* and *F*), the amount of zinc inhibition of extrasynaptic NMDARs is reduced at these frequencies (reduced ZX1 potentiation at higher frequency, Fig. 5*C*). This phenomenon could occur because glutamate diffuses farther than zinc and/or could be the result of faster depletion of zinc compared with glutamate. In either case, this result indicates that, following higher-frequency stimulation and higher levels of glutamate spillover, zinc is less potent in inhibiting extrasynaptic NMDARs.

To determine the origin of zinc that modulates extrasynaptic NMDARs at higher frequencies, we explored the effect of ZX1 application in ZnT3 KO mice at the same higher frequencies of stimulation. We observed that ZX1 potentiated extrasynaptic NMDAR EPSCs at higher frequencies (Fig. 5 *D–F*), in contrast

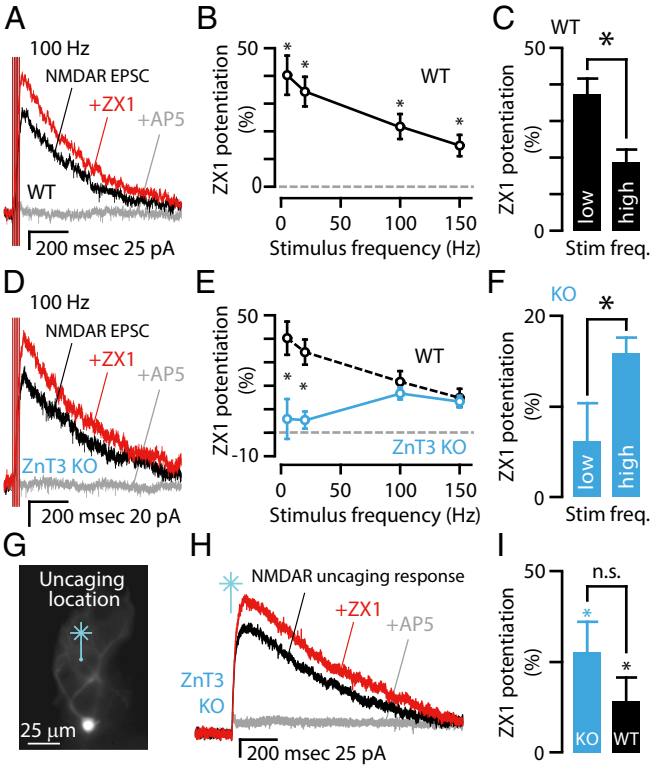

Fig. 5. Synaptic zinc modulation of extrasynaptic NMDARs is frequency-dependent; a pool of ZnT3-independent zinc inhibits extrasynaptic NMDARs activated by high-frequency trains. (*A*) Representative traces from a WT mouse showing that NMDAR EPSCs (black trace) following a 100-Hz stimulus train were potentiated after zinc chelation by 100 μM ZX1 (red trace). AP5 (gray trace) abolished the response, indicating that it was due to NMDAR activation. (*B*) Average graph showing the frequency dependence of NMDAR EPSCs potentiation by zinc chelation in WT mice [n = 8, P < 0.006 for all frequencies vs. control (no ZX1) paired t tests]. (*C*) Group data showing that in WT mice the potentiation of NMDAR EPSCs by ZX1 is significantly larger for NMDARs activated by low-frequency trains (5 and 20 Hz) than for high-frequency trains (100 Hz and 150 Hz; n = 8, P = 0.0001, paired t test). (*D*) Representative traces from a ZnT3 KO mouse showing that NMDAR EPSCs (black trace) following a 100-Hz stimulus train were potentiated by 100 μM ZX1 (red trace); AP5 (gray trace) abolished the response. (*E*) Average graph showing the frequency dependence of NMDAR EPSC potentiation by zinc chelation in ZnT3 KO mice (n = 6, 5 Hz: P = 0.522; 20 Hz: P = 0.20; 100 Hz: P = 0.001; 150 Hz: P = 0.003, paired t tests). For comparison between WT and KO, WT data are replotted from *B*. The difference between WT and ZnT3 KO mice occurred only at low stimulus frequencies, indicated by asterisk [WT (n = 8) vs. KO (n = 6): 5 Hz: P = 0.008; 20 Hz: P = 0.01, t tests, the blue line designates ZnT3 KO]. (*F*) Group data showing that in ZnT3 KO mice the potentiation of NMDAR EPSCs by ZX1 is significantly smaller for NMDARs activated by low-frequency trains (5 and 20 Hz) than for high-frequency trains (100 Hz and 150 Hz; n = 6, low vs. high: P = 0.034, paired t test). (*G*) Epifluorescent image showing the location of glutamate uncaging (the site of UV laser flash) in the molecular layer onto the dendrites of a cartwheel cell in the presence of SR95531 (20 μM), strychnine (1 μM), DNQX (20 μM), and tetrodotoxin (TTX) to prevent action potentials (500 nM, sodium channel blocker). (*H*) Representative traces showing that the NMDAR current (black) was potentiated by the addition of ZX1 (red) and abolished by subsequent addition of AP5 (gray). (*I*) Group data showing that ZX1 increased NMDAR-mediated currents significantly in both ZnT3 KO and WT mice (paired t test for comparisons within genotypes; ZnT3 KO, P = 0.023, n = 5, WT, n = 11, P = 0.007. Wilcoxon rank-sum test for comparison between genotypes, P = 0.21). Error bars represent SEM. Detailed values are given in *SI Material and Methods, Values for Main Figures*.

to the lack of an effect at lower-frequency stimulation in ZnT3 KO mice (Fig. 3 *A–C*). During high-frequency trains, ZX1 potentiated NMDAR EPSCs in WT mice to the same extent as in ZnT3 KO mice (Fig. 5*E*), indicating that the origin of this effect is the tonic, ZnT3-independent (nonsynaptic) zinc. Moreover, this result indicates that, during higher-frequency stimulation, synaptic zinc release did not increase free zinc levels above tonic zinc levels at the locations where most extrasynaptic NMDARs were activated (Fig. 5*E*). We conclude that, during higher-frequency stimulation, glutamate activates extrasynaptic NMDARs at locations not reached by synaptic zinc; the zinc that inhibits these extrasynaptic NMDARs is ZnT3-independent.

Similar to our findings in WT mice, the differential effect of zinc chelation in ZnT3 KO mice during high- and low-frequency stimulation is not due to differences in the proportions of GluN2A vs. GluN2B subunits (Table S1). Because extrasynaptic NMDARs activated during high-frequency trains are inhibited by zinc that is not released from synaptic terminals, we hypothesized that this pool of zinc provides tonic inhibition of these receptors. To confirm that this ZnT3-independent pool of zinc is independent of synaptic release—and is therefore tonic zinc—we bypassed synaptic release by activating NMDARs in ZnT3 KO mice with laser-based glutamate uncaging. When we uncaged glutamate in the molecular layer onto the dendritic arbor of cartwheel cells (Fig. 5*G*), we evoked NMDAR currents that were potentiated by the addition of the zinc chelator ZX1 (Fig. 5 *H* and *I*). This result confirms that non-synaptic—tonic—zinc inhibits NMDARs. In addition, zinc chelation with ZX1 potentiated NMDAR currents to the same degree in WT and ZnT3 KO mice (Fig. 5*I*), further confirming that tonic zinc levels are ZnT3-independent and inhibit NMDARs activated by either glutamate spillover (Fig. 5 *A–F*) or glutamate uncaging (Fig. 5 *G–I*). These results are consistent with our imaging studies, which revealed nanomolar tonic (ZnT3-independent) zinc levels (Fig. 4 *G–I*). Tonic, ZnT3-independent zinc therefore modulates extrasynaptic NMDARs during higher rates of physiologically relevant presynaptic activity. These findings suggest a very general role of zinc even in brain areas that express extrasynaptic NMDARs but do not have synaptic vesicles containing zinc.

Modulation of Extrasynaptic NMDARs by Synaptic and Tonic Zinc Depends on the Rate of Presynaptic Activity. Higher frequencies of presynaptic stimulation increased NMDAR EPSCs because of increased glutamate release and spillover (Fig. 1 *F* and *G*), suggesting that synaptic (ZnT3-dependent) zinc plays a more dominant role in modulating extrasynaptic NMDARs that are closer to synaptic terminals and activated by lower-frequency stimulation (less spillover) (Fig. 5 *B* and *E*). However, tonic (ZnT3-independent) zinc dominates modulation of extrasynaptic NMDARs that are farther away from synaptic terminals and activated by higher-frequency stimulation protocols (more spillover) (Fig. 5*E*). During zinc release, synaptic zinc levels are higher at extrasynaptic sites located closer to synaptic terminals, and tonic zinc levels are higher at extrasynaptic sites located farther away from synaptic terminals.

To test our hypotheses that tonic zinc modulation is preferentially engaged by higher stimulation frequencies and that activation of distant extrasynaptic NMDARs results from larger glutamate spillover, we modified glutamate spillover in ZnT3 KO mice. Our model predicts that blocking glutamate transporters with TBOA will increase glutamate spillover (Fig. 1*F*), facilitating glutamate released with lower-frequency trains to diffuse farther and activate extrasynaptic NMDARs located farther away from synaptic terminals. In the presence of TBOA, therefore, tonic zinc should have an effect on extrasynaptic NMDARs activated by low-frequency stimulation. Consistent with this expectation, in ZnT3 KO mice lacking synaptic zinc, TBOA significantly increased the effect of tonic zinc on extrasynaptic NMDARs activated with low-frequency trains (Fig. 6 *A* and *B*). We interpret this result to be the consequence of increased synaptic glutamate spillover at lower frequencies in the presence of TBOA. An alternative hypothesis is that increased levels of tonic glutamate in the presence of TBOA—not the changes in phasic, synaptic glutamate—may have revealed the effect of tonic zinc at lower frequencies. This hypothesis predicts that TBOA would increase the effect of ZX1 at all frequencies tested and therefore seems unlikely because TBOA did not have any effect on the magnitude of ZX1 potentiation at higher frequencies (Fig. 6*B*). Together, the data support the conclusion that increased spillover of synaptic glutamate unmasks the effect of tonic zinc at lower frequencies. As a result, TBOA reduced

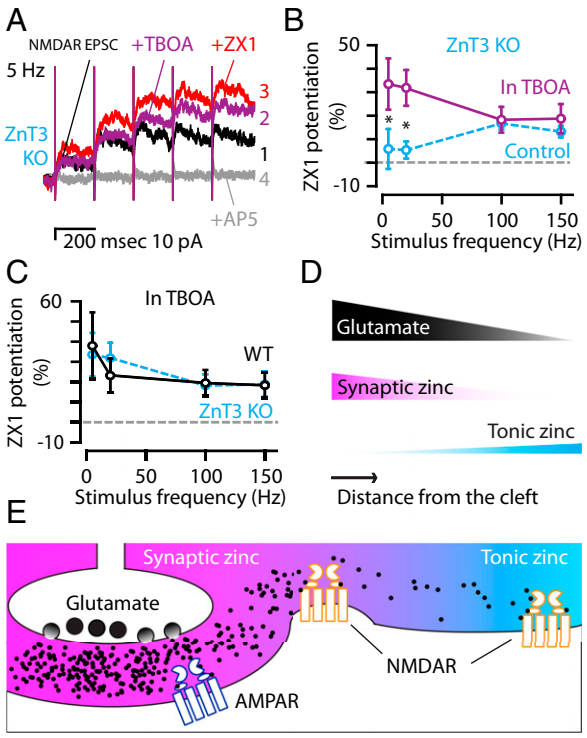

Fig. 6. The amount of glutamate spillover determines the relative strength of synaptic and tonic zinc modulation of extrasynaptic NMDARs; complementary modulation of extrasynaptic NMDARs by synaptic and tonic zinc. (*A*) Representative traces from a ZnT3 KO mouse showing control NMDAR EPSCs in response to 5-Hz stimulation (1: black trace) that were potentiated by the addition of TBOA (2: 50 μM, purple trace), and were further potentiated by zinc chelation with 100 μM ZX1 (3: red trace). AP5 abolished the response (4: gray trace). (*B*) Group data from ZnT3 KO mice showing that TBOA increased the effect of ZX1 only at low stimulus frequencies [ZX1 in TBOA ($n = 9$) vs. ZX1 alone ($n = 6$); 5 Hz: $P = 0.033$; 20 Hz: $P = 0.005$; 100 Hz: $P = 0.399$; 150 Hz: $P = 0.214$, *t* tests]. For comparison, the dotted line represents ZnT3 KO control data (replotted from Fig. 5*E*). (*C*) TBOA abolished the differences in the frequency dependence of zinc modulation between WT and ZnT3 KO mice [compared with ZnT3 KO: WT ($n = 7$), 5 Hz: $P = 0.943$; 20 Hz: $P = 0.811$; 100 Hz: $P = 0.881$; 150 Hz, $P = 0.935$, *t* tests, dotted line: ZnT3 KO data replotted from Fig. 6*B* in TBOA]. (*D* and *E*) Schematic illustrating the gradients of glutamate (black), synaptic zinc (magenta), and tonic zinc (cyan) as a function of the distance from synaptic terminals and their effects on extrasynaptic NMDARs. (*E*) During synaptic release, high levels of glutamate (black dots) near the cleft are accompanied by high levels of synaptic zinc; however, as glutamate moves farther from the cleft, the functional levels of synaptic zinc drop before the functional levels of glutamate. Thus, glutamate activates extrasynaptic NMDARs that are not modulated by coreleased synaptic zinc. These NMDARs are modulated by ZnT3-independent tonic zinc levels, which are lower close to the cleft, but higher at distances farther away from the synapse. Error bars represent SEM. Detailed values are given in *SI Material and Methods, Values for Main Figures*.

significantly the difference of zinc modulation on extrasynaptic NMDAR EPSCs between WT and ZnT3 KO (Fig. 6*C*), suggesting that tonic zinc becomes the main modulator of extrasynaptic NMDARs during conditions that allow increased glutamate spillover.

To summarize, we find that functional glutamate spillover is more extensive than synaptic zinc spillover and can activate extrasynaptic NMDARs not modulated by synaptic zinc (Fig. 6 *D* and *E*). However, under these conditions, tonic zinc is sufficient to provide inhibitory modulation of extrasynaptic NMDARs (Fig. 6*E*). Thus, synaptic and tonic zinc provide complementary modulation of NMDARs, ensuring that phasic activation of extrasynaptic NMDARs is always under the modulatory control of zinc (Fig. 6 *D* and *E*).

Discussion

Synaptic and Tonic Zinc Are Endogenous Modulators of Extrasynaptic NMDARs. Whereas previous studies have shown modulation of synaptic NMDARs by endogenous zinc (7, 8, 12, 28), our results unmask a role for endogenous zinc in tuning the response of extrasynaptic NMDARs. A consensus is emerging that synaptic and extrasynaptic NMDARs are associated with different intracellular signaling pathways and thus serve distinct signaling functions (40–42). For example, synaptic NMDARs contribute to LTP, whereas both extrasynaptic and synaptic NMDARs are required for long-term depression (LTD) (42). Moreover, although still controversial, recent results suggest that, in contrast to the overall neuroprotective roles ascribed to synaptic NMDARs (refs. 40 and 43), but see ref. 42), extrasynaptic NMDAR calcium influx triggers intracellular signaling cascades that can result in mitochondrial damage and cell death (40, 41, 44). In support of this view, pathological up-regulation of extrasynaptic NMDAR activation has been associated with neurodegenerative disorders such as Alzheimer's and Huntington's disease (40, 45, 46). We therefore propose that, by modulating extrasynaptic NMDARs, synaptic zinc may act as an endogenous neuroprotective agent.

Our study identifies a separate pool of zinc that is not ZnT3-dependent and that modulates neuronal excitability via tonic inhibition of extrasynaptic NMDARs. Because recent studies show that ZnT3-independent zinc inhibits spontaneous firing of DCN principal neurons (47), the role of zinc in the mammalian CNS is even more general than previously thought: Zinc may fine-tune neuronal excitability even in brain areas that do not contain synaptic vesicles loaded with zinc.

Although we know that the source of tonic zinc is not ZnT3-dependent in DCN parallel fiber synapses, we do not know its origin. The SLC30 (ZnT) and SLC39 (ZIP) families of zinc transport proteins tightly control cellular zinc levels (48, 49). Although the localization of ZIP and ZnT transporters is less well known, the opposing gradients of synaptic and tonic zinc as a function of the distance from synaptic terminals (Fig. 6*E*) suggest a gradient with lower expression of ZnTs, which export zinc away from the cytosol into organelles or into the extracellular space, in the cleft and higher ZnT expression outside the cleft. Additionally, our results suggest a higher expression of ZIPs, which import zinc into the cytosol from organelles or from the extracellular space, in the cleft and lower ZIP expression outside the cleft. Moreover, the source of ZnT3-independent zinc may be neuronal or nonneuronal. In any case, additional studies are required for identifying the source of tonic, ZnT3-independent zinc as well as the mechanisms underlying the generation of opposing gradients of synaptic and tonic zinc.

When we increased glutamate spillover with TBOA, we found that tonic zinc had a dominant effect over synaptic zinc in inhibiting extrasynaptic NMDARs (Fig. 6). Thus, tonic zinc, which is ZnT3-independent, can play a powerful endogenous neuroprotective role during pathological glutamate clearance, occurring, for example, following ischemia (50, 51). The emergence of tonic zinc as the main modulator under these conditions could also explain the absence of the severe CNS phenotype in ZnT3 KO mice (52) (but see also refs. 53 and 54). We propose that events eliminating extracellular tonic, ZnT3-independent zinc levels may induce more severe CNS pathology than that observed in ZnT3 KO mice.

Our novel ratiometric zinc probe LZ9 allowed us to determine that ZnT3-independent tonic zinc is present in nanomolar-level concentrations sufficient to inhibit extrasynaptic GluN2A-containing NMDARs (Figs. 4–6). Because extrasynaptic NMDARs modulated by tonic zinc are pharmacologically indistinguishable from those modulated by synaptic zinc (Fig. 3*D* and Table S1), we assume that GluN2A-containing NMDARs mediate synaptic zinc inhibition in both cases (7, 19). In our experiments, tonic zinc chelation brought about a ∼15% potentiation of extrasynaptic NMDARs (Fig. 5*F*), indicating that the presence of tonic zinc had caused a ∼13% block of these receptors. At physiological pH, the maximum efficacy of zinc inhibition of GluN2A-containing NMDARs is ∼49% (20). Thus, tonic zinc inhibits extrasynaptic NMDARs to ∼26% of its maximum efficacy. Because the IC_{50} value for zinc binding to GluN2A-containing NMDARs is ∼60 nM (20), we estimate that tonic zinc levels are ∼10 nM. The low nanomolar values of tonic zinc reported by the probe are in good agreement with our electrophysiologically determined estimates (Fig. 4*H*), which are based on the well-established, low-nanomolar sensitivity of endogenous NMDARs. Because low-nanomolar zinc levels enhance the activity of glycine receptors (55, 56), our estimates of low-nanomolar tonic zinc levels are also consistent with recent studies showing that tonic zinc potentiates glycine receptors in DCN principal neurons (47). We are therefore confident that the ratiometric probe is reporting accurate levels of tonic zinc. Although wide-field imaging of bath-applied, extracellular fluorescent zinc probes lacks the spatial and temporal resolution required for quantifying highly localized, rapidly generated, synaptic zinc signals, our ratiometric zinc probe is well suited for measuring tonic zinc levels, which are far less temporally and spatially restricted than synaptic zinc.

Previous electrophysiological studies presented conflicting results describing the ability of ambient, ZnT3-dependent zinc levels to modulate NMDARs in mossy fiber synapses (7, 12). In one study, ZnT3-dependent tonic zinc levels modulated NMDARs in mossy fibers (12), but more recent work reported no effect of ambient zinc on NMDARs in mossy fiber synapses (7). The discrepancy is probably due to the use of CaEDTA (12), which can chelate zinc from nanomolar-affinity zinc-binding sites, and tricine (7), which is unable to chelate zinc from nanomolar-affinity zinc-binding sites (Fig. 2). Our studies, which used the high-affinity zinc chelator ZX1 (Fig. 2), support a role for tonic, but ZnT3-independent, zinc in modulating extrasynaptic NMDARs in the DCN.

Prior studies also reported contradictory results regarding zinc spillover to neighboring synapses in hippocampal slices. One suggested that synaptic zinc may spread from its release site in mossy fibers and provide heterosynaptic modulation of synaptic NMDARs in stratum radiatum (57), whereas another showed a lack of modulation of zinc in stratum radiatum synaptic NMDARs after mossy fiber stimulation (12). The discrepancy may be due to the use of a cell-permeable zinc chelator by Ueno et al. (57) and the extracellular, but sluggish, zinc chelator used by Vogt et al. (12). Our studies, which used the fast extracellular zinc chelator ZX1, support a role for synaptic zinc spillover in modulating extrasynaptic NMDARs in the DCN.

Tonic vs. Phasic Zinc Release. Although previous studies reveal that vesicular zinc is released during neurotransmission (7–9, 12, 13, 58, 59), there remains a controversy about whether released synaptic zinc is free to diffuse, or whether it contributes to the

generation of a tonic level of zinc in the extracellular space (3, 5, 10, 60). Our results in the DCN show that, in response to brief trains of synaptic stimuli, phasic release of synaptic/vesicular zinc modulates extrasynaptic NMDARs. Consistent with our results, previous findings in the DCN also report the requirement of trains of action potentials for zinc-dependent activation of endocannabinoid synthesis and inhibition of probability of release in parallel fiber synapses (13). In mossy fiber synapses, a recent study also suggests that short trains are required for zinc modulation of NMDARs, but this phenomenon was interpreted to be the consequence of slow kinetics of zinc inhibition of GluN2A-NMDAR (7, 61). Importantly, this result contrasts with previous work from the same synapses, where one action potential was sufficient to reveal zinc-mediated NMDAR modulation (8). Our results reveal that, although both tricine and ZX1 can rapidly chelate zinc (Fig. 2*D*), only ZX1 can effectively prevent zinc from binding to high-affinity (nanomolar) sites (Fig. 2 *B* and *E*). The inability of tricine to compete with high-affinity, low-nanomolar zinc-binding sites (Fig. 2*B*) and/or its time-dependent chelating effect (Fig. 2*E*) may explain the inability of this reagent to reveal zinc modulation in NMDAR EPSCs in response to a single stimulus (7). Our results with ZX1 in the DCN show that zinc modulates extrasynaptic, not synaptic, NMDARs—these receptors can be activated by trains of stimuli (Fig. 1*B*) or by a single strong stimulus (Fig. 1*D*) that allows for glutamate spillover to extrasynaptic NMDARs.

In summary, this work establishes synaptic zinc as a neuromodulatory neurotransmitter that modulates the activity of extrasynaptic NMDARs, reveals a ZnT3-independent pool of tonic zinc that also modulates extrasynaptic NMDARs, introduces the ratiometric zinc sensor for measuring extracellular tonic zinc levels, and establishes ZX1 as a most efficient extracellular zinc chelator for studying synaptic zinc.

Materials and Methods

All animal procedures were approved by Institutional Animal Care and Use Committees of the University of Pittsburgh. Methods, data analysis, and statistics are provided in *SI Materials and Methods*.

ACKNOWLEDGMENTS. We thank Dr. Elias Aizenman for many helpful discussions, advice, and technical assistance; Drs. Craig Jahr and Elias Aizenman for comments on this manuscript; and the Auditory Research Group for helpful discussions. This work was supported by NIH Grants T32-DC011499 and F32-DC013734 (to C.T.A.), R01-GM065519 (to S.J.L.), and R01-DC007905 (to T.T.).

1. Paoletti P, Vergnano AM, Barbour B, Casado M (2009) Zinc at glutamatergic synapses. *Neuroscience* 158(1):126–136.
2. Besser L, et al. (2009) Synaptically released zinc triggers metabotropic signaling via a zinc-sensing receptor in the hippocampus. *J Neurosci* 29(9):2890–2901.
3. Kay AR, Tóth K (2008) Is zinc a neuromodulator? *Sci Signal* 1(19):re3.
4. Frederickson CJ, Koh JY, Bush AI (2005) The neurobiology of zinc in health and disease. *Nat Rev Neurosci* 6(6):449–462.
5. Kay AR (2003) Evidence for chelatable zinc in the extracellular space of the hippocampus, but little evidence for synaptic release of Zn. *J Neurosci* 23(17):6847–6855.
6. Nydegger I, Rumschik SM, Kay AR (2010) Zinc is externalized rather than released during synaptic transmission. *ACS Chem Neurosci* 1(11):728–736.
7. Vergnano AM, et al. (2014) Zinc dynamics and action at excitatory synapses. *Neuron* 82(5):1101–1114.
8. Pan E, et al. (2011) Vesicular zinc promotes presynaptic and inhibits postsynaptic long-term potentiation of mossy fiber-CA3 synapse. *Neuron* 71(6):1116–1126.
9. Qian J, Noebels JL (2005) Visualization of transmitter release with zinc fluorescence detection at the mouse hippocampal mossy fibre synapse. *J Physiol* 566(Pt 3):747–758.
10. Ruiz A, Walker MC, Fabian-Fine R, Kullmann DM (2004) Endogenous zinc inhibits GABA(A) receptors in a hippocampal pathway. *J Neurophysiol* 91(2):1091–1096.
11. Frederickson CJ, et al. (2006) Synaptic release of zinc from brain slices: Factors governing release, imaging, and accurate calculation of concentration. *J Neurosci Methods* 154(1-2):19–29.
12. Vogt K, Mellor J, Tong G, Nicoll R (2000) The actions of synaptically released zinc at hippocampal mossy fiber synapses. *Neuron* 26(1):187–196.
13. Perez-Rosello T, et al. (2013) Synaptic Zn2+ inhibits neurotransmitter release by promoting endocannabinoid synthesis. *J Neurosci* 33(22):9259–9272.
14. Frederickson CJ, Howell GA, Haigh MD, Danscher G (1988) Zinc-containing fiber systems in the cochlear nuclei of the rat and mouse. *Hear Res* 36(2-3):203–211.
15. Oertel D, Young ED (2004) What's a cerebellar circuit doing in the auditory system? *Trends Neurosci* 27(2):104–110.
16. Mugnaini E, Morgan JI (1987) The neuropeptide cerebellin is a marker for two similar neuronal circuits in rat brain. *Proc Natl Acad Sci USA* 84(23):8692–8696.
17. Clark BA, Cull-Candy SG (2002) Activity-dependent recruitment of extrasynaptic NMDA receptor activation at an AMPA receptor-only synapse. *J Neurosci* 22(11):4428–4436.
18. Nahir B, Jahr CE (2013) Activation of extrasynaptic NMDARs at individual parallel fiber-molecular layer interneuron synapses in cerebellum. *J Neurosci* 33(41):16323–16333.
19. Paoletti P, Ascher P, Neyton J (1997) High-affinity zinc inhibition of NMDA NR1-NR2A receptors. *J Neurosci* 17(15):5711–5725.
20. Hansen KB, Ogden KK, Yuan H, Traynelis SF (2014) Distinct functional and pharmacological properties of Triheteromeric GluN1/GluN2A/GluN2B NMDA receptors. *Neuron* 81(5):1084–1096.
21. Dingledine R, Borges K, Bowie D, Traynelis SF (1999) The glutamate receptor ion channels. *Pharmacol Rev* 51(1):7–61.
22. Carter AG, Regehr WG (2000) Prolonged synaptic currents and glutamate spillover at the parallel fiber to stellate cell synapse. *J Neurosci* 20(12):4423–4434.
23. Roberts MT, Trussell LO (2010) Molecular layer inhibitory interneurons provide feedforward and lateral inhibition in the dorsal cochlear nucleus. *J Neurophysiol* 104(5):2462–2473.
24. Clements JD, Lester RA, Tong G, Jahr CE, Westbrook GL (1992) The time course of glutamate in the synaptic cleft. *Science* 258(5087):1498–1501.
25. Diamond JS (2001) Neuronal glutamate transporters limit activation of NMDA receptors by neurotransmitter spillover on CA1 pyramidal cells. *J Neurosci* 21(21):8328–8338.
26. Radford RJ, Lippard SJ (2013) Chelators for investigating zinc metalloneurochemistry. *Curr Opin Chem Biol* 17(2):129–136.
27. Buccella D, Horowitz JA, Lippard SJ (2011) Understanding zinc quantification with existing and advanced ditopic fluorescent Zinpyr sensors. *J Am Chem Soc* 133(11):4101–4114.
28. Nozaki C, et al. (2011) Zinc alleviates pain through high-affinity binding to the NMDA receptor NR2A subunit. *Nat Neurosci* 14(8):1017–1022.
29. Legendre P, Westbrook GL (1990) The inhibition of single N-methyl-D-aspartate-activated channels by zinc ions on cultured rat neurones. *J Physiol* 429:429–449.
30. Cole TB, Wenzel HJ, Kafer KE, Schwartzkroin PA, Palmiter RD (1999) Elimination of zinc from synaptic vesicles in the intact mouse brain by disruption of the ZnT3 gene. *Proc Natl Acad Sci USA* 96(4):1716–1721.
31. Chadderton P, Margrie TW, Häusser M (2004) Integration of quanta in cerebellar granule cells during sensory processing. *Nature* 428(6985):856–860.
32. Jörntell H, Ekerot CF (2006) Properties of somatosensory synaptic integration in cerebellar granule cells in vivo. *J Neurosci* 26(45):11786–11797.
33. Traynelis SF, et al. (2010) Glutamate receptor ion channels: Structure, regulation, and function. *Pharmacol Rev* 62(3):405–496.
34. Rachline J, Perin-Dureau F, Le Goff A, Neyton J, Paoletti P (2005) The micromolar zinc-binding domain on the NMDA receptor subunit NR2B. *J Neurosci* 25(2):308–317.
35. Tovar KR, Westbrook GL (2012) Amino-terminal ligands prolong NMDA receptor-mediated EPSCs. *J Neurosci* 32(23):8065–8073.
36. Woodroofe CC, Masalha R, Barnes KR, Frederickson CJ, Lippard SJ (2004) Membrane-permeable and -impermeable sensors of the Zinpyr family and their application to imaging of hippocampal zinc in vivo. *Chem Biol* 11(12):1659–1666.
37. Rubio ME, Juiz JM (1998) Chemical anatomy of excitatory endings in the dorsal cochlear nucleus of the rat: Differential synaptic distribution of aspartate aminotransferase, glutamate, and vesicular zinc. *J Comp Neurol* 399(3):341–358.
38. Wong BA, Friedle S, Lippard SJ (2009) Solution and fluorescence properties of symmetric dipicolylamine-containing dichlorofluorescein-based Zn2+ sensors. *J Am Chem Soc* 131(20):7142–7152.
39. Grynkiewicz G, Poenie M, Tsien RY (1985) A new generation of Ca2+ indicators with greatly improved fluorescence properties. *J Biol Chem* 260(6):3440–3450.
40. Parsons MP, Raymond LA (2014) Extrasynaptic NMDA receptor involvement in central nervous system disorders. *Neuron* 82(2):279–293.
41. Hardingham GE, Bading H (2010) Synaptic versus extrasynaptic NMDA receptor signalling: Implications for neurodegenerative disorders. *Nat Rev Neurosci* 11(10):682–696.
42. Papouin T, Oliet SH (2014) Organization, control and function of extrasynaptic NMDA receptors. *Philos Trans R Soc Lond B Biol Sci* 369(1654):20130601.
43. Wang Y, Briz V, Chishti A, Bi X, Baudry M (2013) Distinct roles for μ-calpain and m-calpain in synaptic NMDAR-mediated neuroprotection and extrasynaptic NMDAR-mediated neurodegeneration. *J Neurosci* 33(48):18880–18892.
44. Hardingham GE, Bading H (2002) Coupling of extrasynaptic NMDA receptors to a CREB shut-off pathway is developmentally regulated. *Biochim Biophys Acta* 1600(1-2):148–153.
45. Milnerwood AJ, et al. (2010) Early increase in extrasynaptic NMDA receptor signaling and expression contributes to phenotype onset in Huntington's disease mice. *Neuron* 65(2):178–190.
46. Li S, et al. (2011) Soluble Aβ oligomers inhibit long-term potentiation through a mechanism involving excessive activation of extrasynaptic NR2B-containing NMDA receptors. *J Neurosci* 31(18):6627–6638.
47. Perez-Rosello T, Anderson CT, Ling C, Lippard SJ, Tzounopoulos T (2015) Tonic zinc inhibits spontaneous firing in dorsal cochlear nucleus principal neurons by enhancing glycinergic neurotransmission. *Neurobiol Dis*, 10.1016/j.nbd.2015.03.012.

48. Huang L, Tepaamorndech S (2013) The SLC30 family of zinc transporters - A review of current understanding of their biological and pathophysiological roles. *Mol Aspects Med* 34(2–3):548–560.
49. Jeong J, Eide DJ (2013) The SLC39 family of zinc transporters. *Mol Aspects Med* 34(2–3): 612–619.
50. Jabaudon D, Scanziani M, Gähwiler BH, Gerber U (2000) Acute decrease in net glutamate uptake during energy deprivation. *Proc Natl Acad Sci USA* 97(10):5610–5615.
51. Choi DW, Rothman SM (1990) The role of glutamate neurotoxicity in hypoxic-ischemic neuronal death. *Annu Rev Neurosci* 13:171–182.
52. Cole TB, Robbins CA, Wenzel HJ, Schwartzkroin PA, Palmiter RD (2000) Seizures and neuronal damage in mice lacking vesicular zinc. *Epilepsy Res* 39(2):153–169.
53. Adlard PA, Parncutt JM, Finkelstein DI, Bush AI (2010) Cognitive loss in zinc transporter-3 knock-out mice: A phenocopy for the synaptic and memory deficits of Alzheimer's disease? *J Neurosci* 30(5):1631–1636.
54. Sindreu C, Palmiter RD, Storm DR (2011) Zinc transporter ZnT-3 regulates presynaptic Erk1/2 signaling and hippocampus-dependent memory. *Proc Natl Acad Sci USA* 108(8):3366–3370.
55. Laube B, Kuhse J, Betz H (2000) Kinetic and mutational analysis of Zn2+ modulation of recombinant human inhibitory glycine receptors. *J Physiol* 522(Pt 2):215–230.
56. Suwa H, Saint-Amant L, Triller A, Drapeau P, Legendre P (2001) High-affinity zinc potentiation of inhibitory postsynaptic glycinergic currents in the zebrafish hindbrain. *J Neurophysiol* 85(2):912–925.
57. Ueno S, et al. (2002) Mossy fiber Zn2+ spillover modulates heterosynaptic N-methyl-D-aspartate receptor activity in hippocampal CA3 circuits. *J Cell Biol* 158(2):215–220.
58. Qian J, Noebels JL (2006) Exocytosis of vesicular zinc reveals persistent depression of neurotransmitter release during metabotropic glutamate receptor long-term depression at the hippocampal CA3-CA1 synapse. *J Neurosci* 26(22):6089–6095.
59. Chorin E, et al. (2011) Upregulation of KCC2 activity by zinc-mediated neurotransmission via the mZnR/GPR39 receptor. *J Neurosci* 31(36):12916–12926.
60. Grauert A, Engel D, Ruiz AJ (2014) Endogenous zinc depresses GABAergic transmission via T-type Ca(2+) channels and broadens the time window for integration of glutamatergic inputs in dentate granule cells. *J Physiol* 592(Pt 1):67–86.
61. Erreger K, Traynelis SF (2005) Allosteric interaction between zinc and glutamate binding domains on NR2A causes desensitization of NMDA receptors. *J Physiol* 569(Pt 2):381–393.